Chapter 7

X-ray Imaging

Authors: Martin Berger, Qiao Yang, and Andreas Maier

7.1 Introduction

In this chapter, the physical principles of X-rays are introduced. We start with a general definition of X-rays compared to other well known rays, e. g., the visible light. In Sec. 7.2, we will learn how X-rays can be generated and how they can be characterized with respect to their energy. The most relevant concept to understand how X-ray imaging works is the behavior of X-rays when they interact with matter. This is outlined in detail in Sec. 7.3. In Sec. 7.4, conventional X-ray imaging is described with a focus on detector types and sources of noise. Finally, we finish this chapter with an overview of well known application areas for X-ray imaging in Sec. 7.5.

7.1.1 Definition of X-rays

X-rays belong to the group of electromagnetic rays, hence, they follow the rules of electromagnetic radiation. Electromagnetic radiation transports en-

A. Maier et al. (Eds.): Medical Imaging Systems, LNCS 11111, pp. 119–145, 2018.
https://doi.org/10.1007/978-3-319-96520-8_7

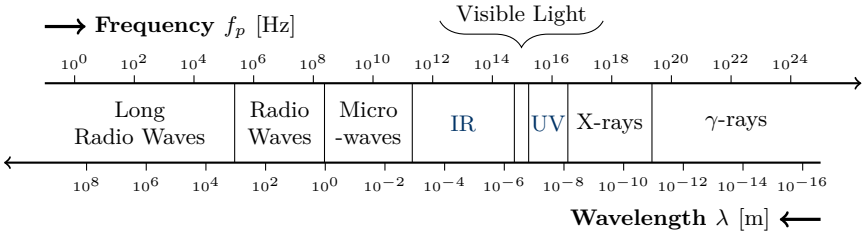

Figure 7.1: Wavelengths and frequencies of the different groups of electromagnetic radiation. X-rays lie in the range of 0.01 nm up to 10 nm.

ergy, also called radiant energy, through space by waves and photons, just as radio waves, the visible light or microwaves. It can either be represented by photons or by a wave model. We will use both representations in the process of this chapter. Radiation can be classified by its wavelength λ_p which is the length of one period of the wave. The wavelength can also be represented by frequency f_p and the waves propagation speed, i. e., the speed of light c_0.

$$\lambda_p = \frac{c_0}{f_p} \tag{7.1}$$

In Eq. (7.2) the energy of photons is given, where h denotes Planck's constant ($\approx 6.626\,069 \times 10^{-34}\,\mathrm{J\,s}$) and c_0 is the speed of light ($\approx 2.997\,92 \times 10^{5}\,\mathrm{m\,s^{-1}}$). The energy is directly related to the photon's wavelength λ_p or its frequency f_p and is given by the unit electron volt [eV]. We can easily obtain that the photon energy is proportional to its frequency and inverse proportional to its wavelength, that means the higher its frequency, the higher its energy.

$$E_p = \frac{h\,c_0}{\lambda_p} = f_p\,h \tag{7.2}$$

The energy is also used to characterize electromagnetic radiation into different groups, i. e., radio waves, microwaves, infrared (IR), visible light, ultraviolet (UV) light, X-rays and γ-rays. Fig. 7.1 shows these groups with respect to their characteristic ranges of frequency and wavelength. Note that the wavelength of most X-rays lies in the range of 0.01 nm up to 10 nm. This corresponds to an energy range of 100 keV down to 100 eV.

As visible light, X-rays loose a certain amount of energy when they pass through different materials. The energy loss depends on the absorption behavior of the material. For example if X-rays pass through 10cm of water, they loose less energy than if they would pass trough 10cm of bone. The reduction of energy is caused by absorption which is the main principle of traditional X-ray imaging. Generally speaking, X-ray radiography measures the amount of energy loss. Because this energy loss differs for the different materials, we can see a certain contrast in the image. For example an X-ray

image shows high intensities for soft tissue and lower intensities where the X-rays passed through bones. Note that the absorbed energy is directly related to the dose that is delivered to the patient during an acquisition.

7.1.2 History and Present

Discovery of X-rays

X-rays have been discovered by Wilhelm Conrad Röntgen in Würzburg, Germany. On November 8, 1895, he conducted experiments including Crookes tubes, which are typically used to visualize streams of electrons. He further used a fluorescent screen and covered the actual tube with black cardboard. When moving the fluorescent screen away from the tubes opening he realized that there was still a glimmer visible on the fluorescent screen, which had to be the result from radiation that passes through the black cardboard. Additional experiments where he replaced the cardboard with denser materials, e. g., books led to the same observation. After that, he began a systematic study of the new radiation, which he then named "X"-rays. One of the first acquired X-ray images is shown in Fig. 7.3. It depicts the hand of Röntgen's wife, where we can clearly see the ring she was wearing on her annular finger. It is not to be confused with a similar image depicted in Fig. 7.4 which was taken later in January of 1896.

Only on December 28, 1895, about six weeks after the first discovery, Röntgen submitted the first known article on X-rays entitled "Über eine neue Art von Strahlen" (On a new type of rays) which shows first reports on the absorption properties of different materials, e. g., paper, wood and also metal. Already in January 1896, Röntgen demonstrated his discovery to the German medical-physical society. Creating an X-ray of Albert von Kölliker's hand (cf. Fig. 7.4) – a well-known anatomist at that time – in front of the audience immediately convinced Röntgen's colleagues of the utility of his invention. For his groundbreaking discovery, Röntgen received the first awarded Nobel Prize in Physics in 1901. In Fig. 7.2, we can see an image of Wilhelm Conrad Röntgen, taken for the Nobel-Prize committee. The actual commercial implementation was performed by others (cf. Geek Box 7.1).

X-rays Today

Today, X-rays are routinely used in diagnostic but also in interventional medical imaging around the globe. Also in industry, X-rays are often the method of choice, for example to test for very small cracks in metal parts in the field of non-destructive testing. In medical imaging, a variety of applications have been developed that go far beyond simple radiographic imaging. For example

Geek Box 7.1: Commercial Success of X-rays

Röntgen donated his discovery to humanity and never made any commercial profit. He also never filed a patent for his invention. The actual commercial roll-out of the technology was performed by several small companies:

- In 1877, *Erwin Moritz Reiniger*, a former employee of *Friedrich-Alexander-University Erlangen-Nuremberg*, Germany, founded a small workshop right next to the university with the aim of producing batteries and physical measurement devices. In 1886, *Max Gebbert* and *Karl Friedrich Schall* joined Reiniger's workshop founding the *Vereinigte Physikalisch-Mechanische Werkstätten Reiniger, Gebbert & Schall — Erlangen, New York, Stuttgart*. In 1896, they switched the focus of production to X-ray tubes. Over the years this small company grew and is today known under the name *Siemens Healthineers AG*.
- *Victor Electric Company* was founded in 1893 by C. F. Samms and J. B. Wantz in a basement in Chicago, United States of America, with the aim of producing physical measurement gear. In 1896, they also began with the production of X-ray tubes. Also this small company turned out to be very commercially successful and is today known as *General Electric Healhcare*.
- In 1896, *C. H. F. Müller* developed the first commercial X-ray tube in Hamburg, Germany, in cooperation with the *University Clinic Hamburg-Eppendorf*. In 1927, the company was bought and is today an integral part of *Philips Medizin Systeme GmbH*.

fluroscopy allows for real time X-ray sequences which are often inevitable in minimally invasive interventions. Further, digital subtraction angiography (DSA) provides an effective tool to visualize even small vessel structures. In the 1970s, the step to CT was done which now allows to visualize the complete human body in three dimensions. Another point of rapid development is the awareness that X-rays can also be harmful. High energies emitted to the body during an X-ray acquisition can lead to ionization. That means the radiation changes the atomic structure of the tissue which can potentially lead to an increased risk for the development of cancer. Here, deoxyribonucleic acid (DNA) becomes damaged by the radiation. In most cases, the DNA will be repaired by the cell itself. Yet, the repair process sometimes fails which in some cases leads to an unregulated division of cells that might result in cancer. X-ray-based foot scanners where still in use to measure foot sizes in shoe stores until the 1970s. Nowadays, the majority of people is aware of the risk posed by X-rays and the transmitted patient dose during X-ray scans

Figure 7.2: Wilhelm Conrad Röntgen

Figure 7.3: One of the first X-rays, taken from Wilhelm Röntgen of his wifes hand.

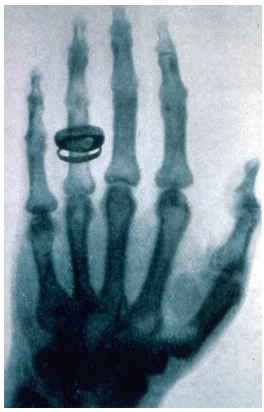

Figure 7.4: Image taken in 1896 showing Albert von Kölliker's hand.

has been significantly reduced in the past decades[1]. In Fig. 7.5, we can see an X-ray taken in mammography which typically uses low-energy X-rays to increase soft-tissue contrast. Another example is shown in Fig. 7.6, where we can see an X-ray image taken from the thorax, i. e., the chest, of a patient.

7.2 X-ray Generation

A classical X-ray tube is depicted in Fig. 7.7. An X-ray tube is basically an evacuated tube made of glass with a cathode and a solid metal anode in it. Thermionic emission occurs by the heated filament at the cathode. Heat induced electrons e^- are produced because the thermal energy applied to the filament material is larger than its binding energy. Then, the electrons are accelerated by the tube's acceleration voltage between the negative cathode and the positive anode. When those fast electrons hit the anode, they are decelerated and deflected by the electric field of the atoms of the anode material. Any acceleration of loaded particles results in electromagnetic waves. So does the slowing down, i. e., the negative acceleration, of the electrons in the metal anode. It generates X-rays.

The anode is tilted by a certain angle to direct the emerging X-rays in the right direction. Typically each electron is slowed down or deflected several times so it causes the creation of several photons. However it can also happen

[1] Although being full of mistakes (as claimed by the authors), a good overview on radiation doses is found at https://xkcd.com/radiation/.

Figure 7.5: Example of a breast X-ray. Note the clearly visible structures in the soft-tissue.

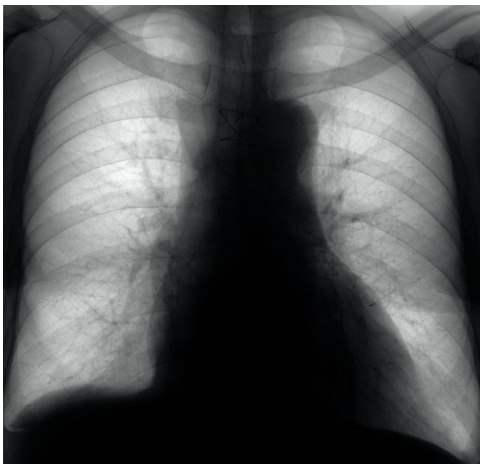

Figure 7.6: Example of an X-ray taken from the chest of a patient.

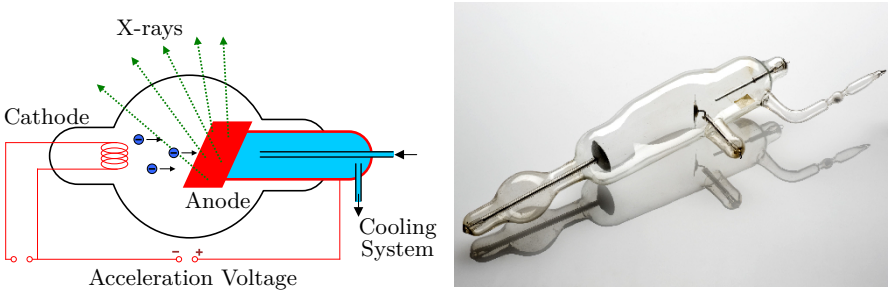

Figure 7.7: Vacuum X-ray tube: The image on the left shows a schematic how electrons are accelerated from the cathode to the anode to genereate X-ray photons. The image on the right shows a historic vacuum X-ray tube. Image provided by Science Museum, London, Wellcome Images under Creative Commons by-nc-nd 2.0 UK.

that an electron loses all its velocity and thus its energy in one step. In this case, only one photon containing the complete energy of the electron is created.

The production of X-rays is caused by two different processes as shown in Fig. 7.8. First, if the electron interacts with an inner-shell electron of the target, characteristic X-radiation can be produced. This kind of X-rays results from a sufficiently strong interaction that ionizes the target atom by a total removal of the inner-shell electron. The resulting “hole” in the inner-shell is

filled with an outer-shell electron. The transition of an orbital electron from an outer-shell to an inner-shell is accompanied by the emission of an X-ray photon, with an energy equal to the difference in the binding energies of the orbital electrons involved. Therefore, the characteristic radiation produces a line spectrum, or discrete spectrum. Obviously, this kind of radiation is material dependent. Both the production of characteristic X-rays as well as thermal energy involve interactions between the accelerated electrons and the electrons of the target material.

Another type of interaction in which the electron can lose its kinetic energy delivers the second process of X-ray production, caused by the interaction of the electron with the nucleus of a target atom. As the colliding electron passes by the nucleus of an anode atom, it is slowed down and deviated in its course, leaving with reduced kinetic energy in a different direction. This loss in kinetic energy reappears as an X-ray photon. This type of X-rays is called Bremsstrahlung, where "bremsen" is the German verb for slowing down. The amount of kinetic energy that is lost in this way can vary from zero to the total incident energy. While the characteristic radiation results in a discrete X-ray spectrum of characteristic peaks, the Bremsstrahlung provides a continuous spectrum. The number of X-rays emitted decreases rapidly at very low photon energies. The spectrum of a tungsten source is given in Fig. 7.8. In medical imaging, very low energies of an X-ray spectrum are typically removed prior to an interaction with the patient by using a thin metal plate which is placed between the patient and the X-ray source. The reason for this is that almost all of the low energy photons would be absorbed by the patient, thus, leading to an increased patient dose without a substantial improvement of image quality. The metallic plate is also called X-ray filter, which is not to be confused with the mathematical filters used for image processing.

7.3 X-ray Matter Interaction

X-rays have the ability to penetrate matter, yet, the amount of penetrating X-ray photons is material-dependent. Their ability to penetrate human tissue is in fact the reason why they can be used to get information on internal organs. Different tube voltages between the cathode and the anode produce higher or lower energy X-ray spectra. In the energy range that is used for medical imaging, there are three kinds of relevant interactions that can occur when X-rays pass through matter:

- interaction with atomic electrons,
- interaction with nucleons,
- interaction with electric fields associated to atomic electrons and atomic nuclei.

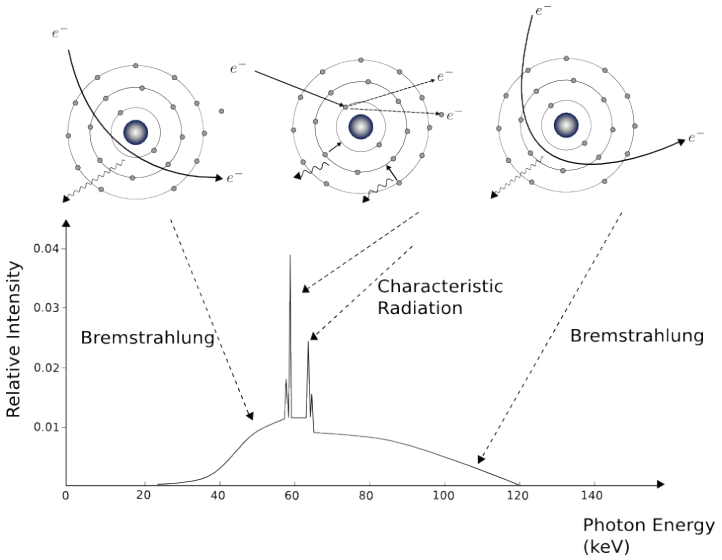

Figure 7.8: X-ray spectrum of a tungsten tube. The peaks correspond to the characteristic radiation; the continuous part of the spectrum represents the Bremsstrahlung.

Consequently, the X-ray photons either experience a complete absorption, elastic scattering or inelastic scattering.

The interaction that is used for medical imaging consists of a reduction of radiation intensity which is nothing else than a reduction of the number of photons that arrive at the detector. That process is usually referred to as attenuation. There are several different physical effects contributing to attenuation, including a change of the photon count, photon direction, or photon energy. All of these effects have in common that they are based on an interaction between single photons and the material that they are passing through and that the attenuation induced by each of them is highly energy-dependent. Sec. 7.3 shows an overview on the different relevant effects. Note that pair production is not relevant for typical diagnostic X-ray energies. To produce a positron and an electron, the photon's energy must exceed at least $2 \times 511\,\mathrm{keV}$.

7.3.1 Absorption

When a monochromatic X-ray beam traverses a homogeneous object with absorption coefficient μ, according to Lambert-Beer's law, the observed intensity I is related to the intersection length of the object x and the ray:

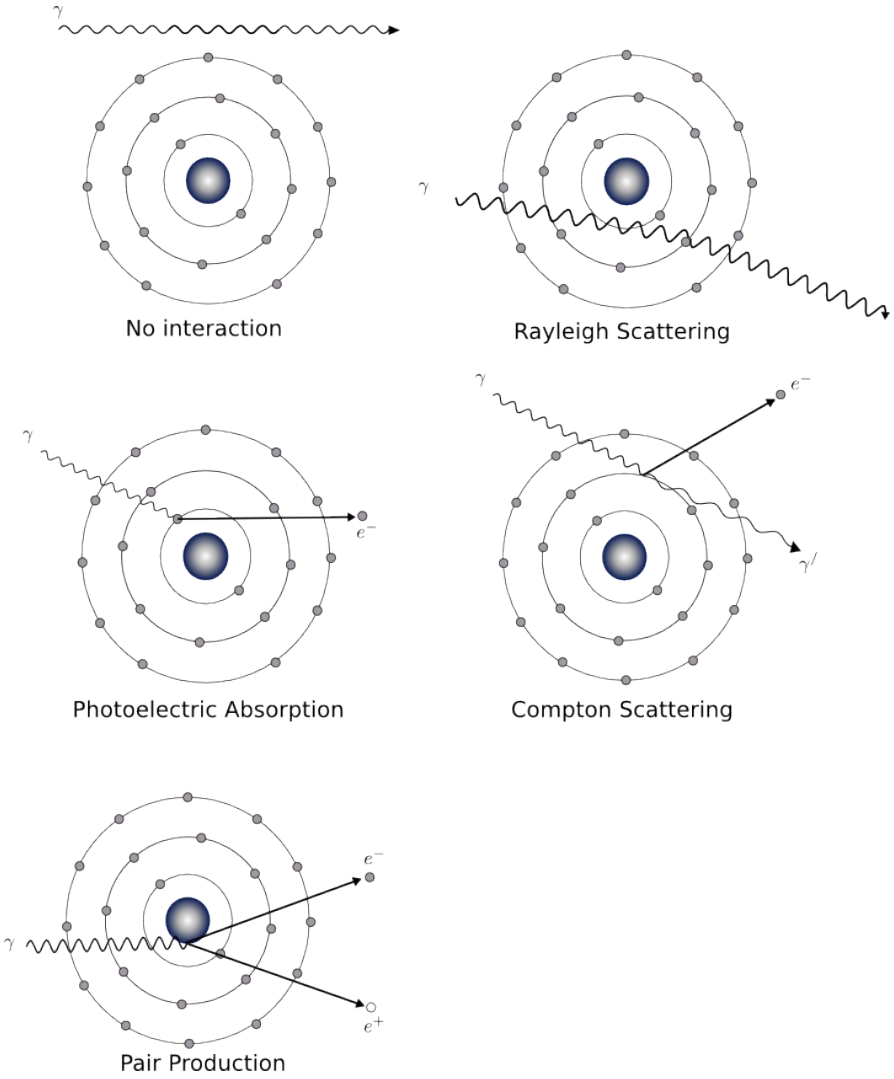

Figure 7.9: Principles of photon-matter interactions.

$$I = I_0 \cdot e^{-\mu x} \quad . \tag{7.3}$$

Here, I_0 is the X-ray intensity at the X-ray source. A derivation is found in Geek Box 7.2.

In X-ray CT, the fractional transmitted intensity I/I_0 is used to measure a large number of ray paths through the object. The logarithm of this ratio is used to obtain a set of line integrals as an input to reconstruction algorithms.

Geek Box 7.2: Lambert-Beer's Law

The radiation intensity decreases which leads to an ordinary linear and homogeneous, first order differential equation with constant coefficient

$$\frac{dI}{I} = -\mu \mathrm{d}x \ .$$

I is the intensity of the incident radiation, dx is the thickness of the material and μ is the material attenuation coefficient. μ mainly consists of contributions from the photoelectric absorption effect and the Compton scattering. If we take the integral on both sides we obtain

$$\int_0^x \frac{dI(x)}{I(x)} \mathrm{d}x = -\int_0^x \mu \mathrm{d}x$$
$$\log I(x) - \log I(0) = -\mu x \ .$$

To solve the logarithms in the equation, we take exponential of both sides. Thus, the equation can be rewritten as

$$I(x) = I(0) \cdot e^{-\mu x} \ .$$

In general, we can define I_0 as the energy of the incident beam and I as the energy after the beam traversed through material with thickness x.

When the ray passes through inhomogeneous objects, factor $\mu(x)$ is the linear attenuation coefficient at each point on the ray path

$$-\ln \frac{I}{I_0} = \int \mu(x) \mathrm{d}x \ . \tag{7.4}$$

However, in practical setups, the emitted X-ray photons have various energies, resulting in polyenergetic energy spectra as shown in Fig. 7.8. The measured intensity of a polychromatic beam I on the detector can be written as the sum of monochromatic contributions for each energy E in the X-ray spectrum ($E \in [0, E_{max}]$). The attenuation coefficient μ is also energy dependent. When polychromatic X-rays are taken into account, we get

$$I = \int_0^{E_{\max}} I_0(E) \exp\left(-\int \mu(x, E) \mathrm{d}x\right) \mathrm{d}E \tag{7.5}$$

where $I_0(E)$ is the normalized energy spectrum, i. e., $\int I_0(E) \mathrm{d}E = 1$.

7.3.2 Photoelectric Effect

The photoelectric effect was originally described by Einstein under the establishment of the quantized nature of light. It describes a situation in which the incident X-ray photon energy is larger than the binding energy of an electron in the target material atom. The incident X-ray photon gives up its entire energy to liberate an electron from an inner-shell. The ejected electron is called photoelectron. The incident photon then ceases to exist. The photoelectric effect often leaves a vacancy in the inner shell of the atom, where the ejected electron was previously located. As a result, the "hole" created in the inner-shell is filled by an outer shell electron. Since the outer shell electron is at a higher energy state, a characteristic radiation occurs. Therefore, the photoelectric effect produces a positive ion, a photoelectron, and a photon of characteristic radiation. For tissue-like materials, the binding energy of the K-shell electrons is very small. Thus, the photoelectron acquires essentially the entire energy of the X-ray photon.

7.3.3 Compton Scattering

The second type of matter interaction is the Compton scattering, which is named after Arthur Holly Compton, who received the Nobel Prize in 1927 for his discovery. For high X-ray energies, Compton scattering is the most dominant interaction mechanism in tissue-like materials. The energy of the incident X-ray photon is considerable higher than the binding energy of the electron. As a result, the incident X-ray photon strikes an electron and ejects the electron from the atom. In Compton scattering, the incoming photon is deflected or scattered through an angle θ with partial loss of its initial energy. The incident photon transfers a portion of its energy to the electron, which is so called "recoil electron", or Compton electron. Therefore, the interaction produces a positive ion, a "recoil electron", and a scattered photon. The scattered photon may be deflected at any angle from 0 to 180 degree. After Compton interaction, most of the energy is retained by the scattered photon, corresponding to a small deflection angle.

7.3.4 Rayleigh scattering

Rayleigh scattering is a coherent process and is the predominant kind of scattering at low X-ray energies. It is caused by an interaction of the incident wave with several, usually outer shell electrons. A very low energy photon interacts with bounded orbital electrons of the atom. No ejection occurs, but the electrons and thus the whole atom is set to vibration with respect to the

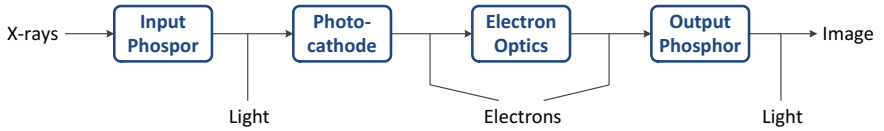

Figure 7.10: Schematic principle of an image intensifier detector. The X-rays are first converted to light, which is converted to electrons. An optic accelerates the electrons towards a fluorescent screen which converts the electrons to light, which eventually results in an image.

incident photon's wavelength. The excess energy from the vibrating electron transfers to an electromagnetic photon which has the same wavelength but possibly a different direction than the incident photon. In this interaction, electrons from the material's atom are not ejected and no energy is converted into kinetic energy, thus, no ionization occurs. Rayleigh scattered photons are mostly emitted in a forward direction with respect to the incident photon's direction. For X-rays used for imaging, the contribution of Rayleigh scattering to total attenuation is usually small compared to other contributions.

7.4 X-ray Imaging

In the previous sections, the concepts of X-ray generation and also their interaction behavior with matter has been outlined. In this section, we will now focus on different detection methods used to convert the X-rays that have passed the patient to an actual image. Unlike the old X-ray films, which use X-rays directly to change the chemical properties of the X-ray film material, the modern detection systems first convert the X-rays to light and eventually to electrons.

7.4.1 Image Intensifiers

X-ray image intensifiers are vacuum tubes that are used to convert X-rays into visible light, i. e., an image. The schematic principle of this process is shown in Fig. 7.10. First, the incoming X-ray photons are converted to light photons using a phosphorus material called the input phosphor. The produced light is further converted to electrons by exploiting the photoelectric effect inside a photocathode. These electrons are then accelerated and focused towards the output phosphor using an electron optic system. In the output phosphor, the electrons are converted back to visible light which can then be captured by film material or television camera tubes.

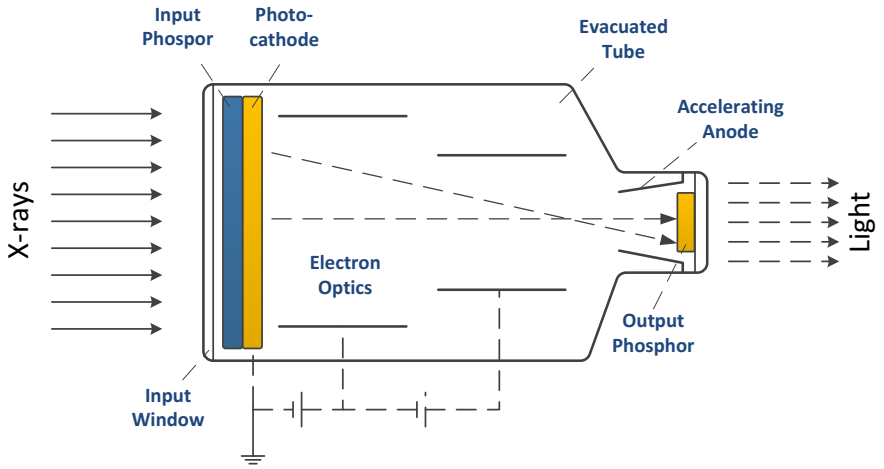

Figure 7.11: Detailed principle of an image intensifier detector. The X-rays are first converted to light, which is converted to electrons. An optic focuses the electron beam to a fluorescent screen or film material which converts the electrons to light, i. e., the image.

Before the introduction of image intensifiers in the late 1940s, fluoroscopic detection system consisted of only one phosphorus material where X-rays have been directly converted to light. However, the mismatch between the high amount of needed X-ray quanta and the low amount of emerging visible light quanta led to very dark images and high radiation exposure. Thus, the radiologists had to view the images in dark surroundings and after a certain time of dark-adaptation of their eyes. The biggest advantage of image intensifier systems is that the brightness of the output image was now adjustable by the amount of acceleration supplied by the electron optics. Modern X-ray image intensifiers have an input field diameter of about 15 to 57 cm. They are characterized by conversion factors that indicate how efficient X-rays are transformed to visible light.

7.4.1.1 Function

A more detailed overview of the individual parts of an image intensifier is given in Fig. 7.11. First the the incoming X-rays pass through the **input window** which typically consists of a convex shaped aluminum plate with a thickness of a approximately 1 mm. The convex shape is used to enhance mechanical stability but also to reduce the distance to the patient which effectively increases the useful entrance field size.

After passing through the input window, the X-rays hit the **input phosphor** used to convert X-ray photons to light photons. The generated light photons trigger a photoelectric effect in the **photocathode** which then emits (photo-)electrons. The input phosphor and the photocathode are typically layered to one piece. Starting with the input phosphor that consists of another aluminum plate coated with the phosphor layer, followed by an intermediate layer and the photocathode layer.

Let us focus on the input phosphor layer in more detail. One important property that influences the efficiency of the input phosphor layer is its thickness. The thicker the phosphor layer, the higher is its absorption, thus, more X-ray photons are absorbed and converted to light. Hence, less X-ray photons are required which reduces radiation exposure to the patient. However, with increasing thickness also more light photons become scattered within the phosphor layer which effectively reduces the spatial resolution.

Another property that is used to increase conversion factors is the chemical composition of the input phosphor material and its resulting mass attenuation coefficient. Ideally, the input phosphor's attenuation coefficient is adjusted to the residual incoming X-ray spectrum. Initially, zinc-cadmium sulfide (ZnCdS) has been used as phosphoric material, which has been replaced by cesium iodide (CsI) in modern detector systems. The advantages of CsI over ZnCdS are twofold. In Fig. 7.12 we illustrate the mass attenuation coefficient of CsI (dashed, dark blue line) and ZnCdS (dotted, light blue line) w. r. t. the photon energy. Additionally, the estimated spectral distribution of a typical X-ray spectrum after transmission through the patient is depicted as solid, orange line. The higher the overlapping area between attenuation characteristics and residual X-ray spectrum, the better its conversion efficiency. We can clearly see that the mass attenuation coefficient of CsI matches better to the expected residual X-ray spectrum and is thus favorable.

Additionally, the manufacturing process of CsI allows to build the phosphor layer as a collection of small and local cylindrical structures as indicated in Fig. 7.14. The cylindrical wires act as optical fibers which can steer the emitted light to the photocathode with a high spatial accuracy. Thus, scattering of the light photons within the phosphor material can be drastically reduced. In modern detectors, the input phosphor is about 300 µm to 500 µm thick and can absorb up to 70 % of the incoming X-ray photons. A single 60 keV X-ray photon can create up to 2600 light photons, where approximately 62 % reach the photocathode.

The **photocathode** layer typically consists of antimony-cesium ($SbCs_3$). Similar to the input photon layer, the incoming light should fit to the sensitivity spectrum given by the photocathode. Fig. 7.13 shows the sensitivity spectrum of an $SbCs_3$ photocathode, together with the characteristic light spectra emitted from a CsI as well as a ZnCdS phospor layer. We can see that also here CsI seems to produce a light spectrum that matches better to the photocathode, hence, leading to a higher conversion efficiency from light photons to electrons.

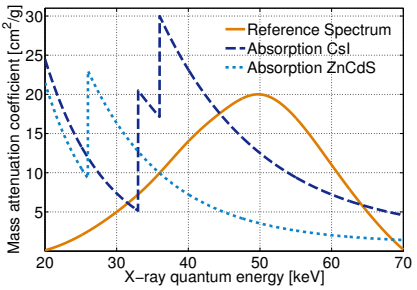

Figure 7.12: Mass attenuation coefficient of CsI and ZnCdS and the estimated X-ray spectrum after transmission through the patient.

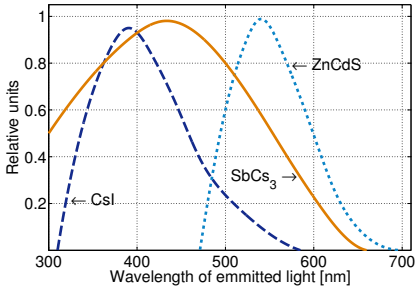

Figure 7.13: Sensitivity of an $SbCs_3$ photocathode and characteristic light spectra emitted from a CsI as well as a ZnCdS phospor layer.

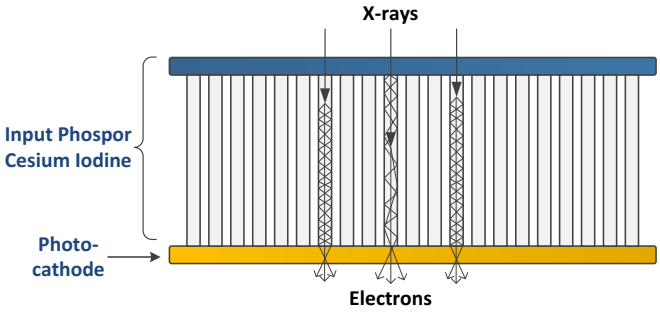

Figure 7.14: Cesium-iodine layer has cylindrical structure and acts as optical fibers. Thus, the scattering of the light photons is reduced significantly.

After the electrons leave the photocathode, they are accellerated by the **anode** as shown in Fig. 7.11. Moreover, the accelerated electrons are focused onto the output phosphor using electrostatic fields produced by the **electron optic**. No additional electrons are induced into the system by this process, the existing electrons are merely accelerated and deflected. The increase of kinetic energy that originates of the acceleration process results in a higher number of light photons that are emitted when the electrons hit the **output phosphor**. Hence, the intensity or brightness of the output phosphor can be altered by a regulation of the acceleration voltage. The output phosphor consists typically of silver-activated zinc-cadmium sulfide (ZnCdS:Ag) and is very thin (4 µm to 8 µm). About 2000 light photons are generated for a single 25 keV electron. Due to the fact that one electron is emitted by one light photon in the photocathode, this also represents an increased brightness by a factor of 2000.

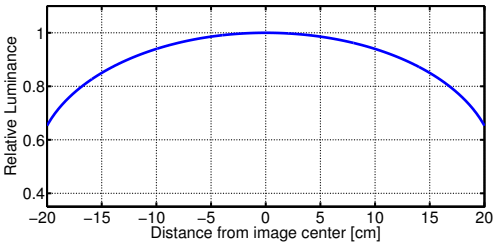

Figure 7.15: Vignetting artifact, i. e., luminescence drops at image periphery.

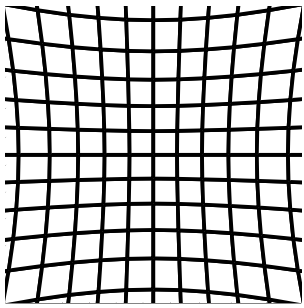

Figure 7.16: Distortion artifacts due to external electric or magnetic field.

7.4.1.2 Known Problems

Besides common limitations that all imaging systems share, e. g., spatial resolution and contrast ratio, image intensifier systems are most known for vignetting and distortion artifacts. Vignetting, as described in Fig. 7.15, describes a drop in brightness that occurs at the outer parts of the screen. It is caused by light scattering that deflects light photons in the output phosphor from the outer part of the phosphor to the inside. However, no scattering occurs from completely outside the material to the outer regions of the phosphor, yielding an increased brightness at the central regions. Another common artifact is image distortion as indicated in Fig. 7.16. It is known that the electron optics of image intensifiers is susceptible to external magnetic or electric fields. Even the earth's magnetic field causes considerable distortions in the output image. To correct for distortion artifacts, regular calibration is needed where the distortion field is estimated by measuring predefined calibration objects. The distortion can be corrected by either adjusting the electron optics accordingly or by subsequent image processing in case the images have been digitized.

7.4.2 Flat Panel Detectors

In the recent years, flat panel detector (FPD) became the state-of-the-art in X-ray detector technology for radiography, angiography, and C-arm CT applications. They were first introduced in the mid 1990s and their main advantages are a direct digital readout of the X-ray image and an increased spatial resolution. Flat panel detectors can be categorized into direct and indirectly conversion FPDs.

Indirect Conversion FPDs

Similar to the image intensifier system discussed in the previous section, the FPD still converts X-rays to light photons by using a layer of cesium iodide (CsI). Also the tubular structure of the CsI is identical to the input layer of an image intensifier system as shown in Fig. 7.14. The major difference are the subsequent detection steps. Image intensifiers make use of a further conversion of light photons to electrons which are then accelerated to increase and control illumination. This additional conversion step is not necessary for flat panel detectors. Instead a matrix of photodiodes is directly attached to the CsI layer and converts the emitted light photons to an electric charge which is then stored in capacitors for each pixel. Each pixel also contains a thin-film transistor (TFT) which acts as small "switch" used for the readout of the stored charges.

Direct Conversion FPDs

Instead of an explicit conversion to light photons, direct conversion FPDs have a homogeneous layer of X-ray sensitive photoconducters on the TFT matrix. The top layer is a high-voltage bias electrode that builds an electric field across the photoconductor. If X-rays are absorbed by the photoconductor, so called charge-carriers are released, i. e., electron-hole pairs. These pairs are then separated to negative and positive charges and transported to the pixel's electrodes by the global electric field. Positive charges travel to the bottom of the individual pixel electrodes where they are stored in capacitors.

Data Readout and Properties

For both the indirect but also the direct conversion FPDs, the readout of the pixels is done row-wise using a certain readout frequency. A row is selected by "switching on" the TFTs of this row's pixels, i. e., by applying a voltage to the gate of the TFTs. The stored charges of each pixel are directed to a charge integrating amplifier and subsequently converted to a digital representation. These digital pixel values are serialized and transferred over a bus system to the imaging computer. Common FPDs for medical imaging can have a side length of up to 40 cm and a pixel size of about 100 µm to 150 µm. They are available in quadratic but also in wide formats. The analog to digital conversion uses a quantization of 12 to 16 Bit. To increase the signal to noise ratio multiple pixels are often combined to a bigger pixel during the readout process, which is also known as binning. Typical binning modes are 2x2 or 4x4 binning, reducing the image size by a factor of 2 or 4, respectively. Because binning does not require any additional time, the frame rate increases by the binning factor. Frame rates typically vary between 7.5 and 30 frames

per second, depending on the medical application, dose requirements, and binning factors.

Major advantages of flat panel detectors are a significant reduction of space and weight needed for the detection unit. This may sound trivial but the benefit becomes more clear when we consider that space is typically limited, especially in an interventional environment and that increased weight is directly related to rotation speeds of CT or C-arm CT devices. Another advantage is the robustness against (moderate) electrical and magnetic fields, which posed a huge problem for image intensifiers. Moreover, the images are directly available in digital form, which makes patient handling and data storage more efficient.

7.4.3 Sources of Noise

There are two types of undesirable effects in medical imaging systems: probabilistic noise and artifacts. Similar to noise, artifacts are image degradations that also find their source in physical effects during the scan. However, the difference to noise is that when a scan is repeated using the exact same object and scan parameters, artifacts are reproduced exactly whereas noise effects will change based on a probabilistic scheme. Some artifacts, for example, distortion and vignetting, have already been shown in the section Sec. 7.4.1 on image intensifier detectors. In the following, we focus on the sources and propagation of noise in X-ray imaging.

As illustrated in Fig. 7.17, there are different states of an X-ray photon. Each step in this chain follows either a Poisson distribution (cf. Geek Box 7.3) or a binomial distribution (cf. Geek Box 7.4). In Fig. 7.18, we show both distributions in comparison. The X-ray photon generation process (cf. Geek Box 7.5) follows a Poission distribution. The matter interaction and the detection step (cf. Geek Box 7.6) follow a binomial distribution. Both processes interact along the path of the X-ray (cf. Geek Box 7.7) resulting in yet another Poisson distribution. As such Lambert-Beer's law also has a probabilistic interpretation (cf. Geek Box 7.8) and every observation on the detector is Poisson distributed in the monochromatic case.

A common quality measure for imaging is the signal-to-noise ratio (SNR). It is not uniquely defined over different fields of applications. In X-ray imaging it makes sense to use the definition based on statistics, i. e.,

$$SNR(\mathcal{N}) = \frac{\bar{n}}{\sigma} = \frac{E(\mathcal{N})}{\sqrt{E((\mathcal{N} - \bar{n})^2)}} \ . \tag{7.6}$$

For random variables $\mathcal{N}$ that follow a normal distribution, $\bar{n}$ is the mean value and σ represents the standard deviation. More generally speaking, the two variables define the first moment ($\bar{n}$) and the second central moment (σ)

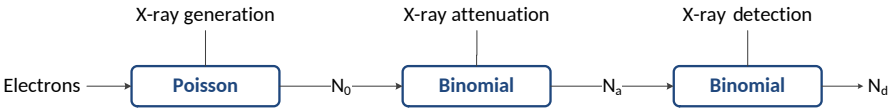

Figure 7.17: Overview of noise related processes in X-ray imaging.

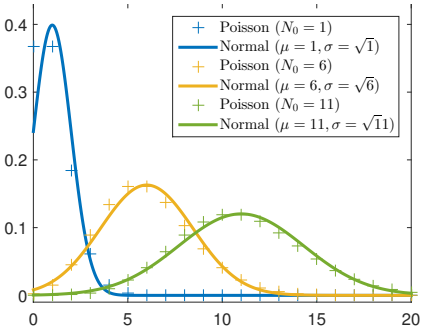

(a) Mass distribution functions of Poisson distributions with varying expectation value N_0, plus their Gaussian counterparts.

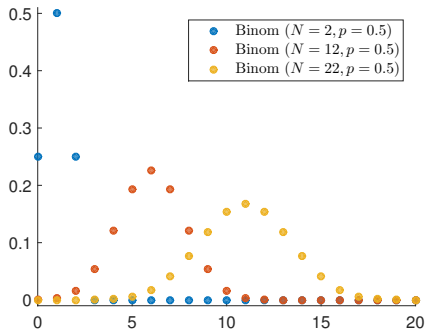

(b) Mass distribution functions of binomial distributions with varying number of trials N and fixed probability $p = 0.5$.

Figure 7.18: Mass distribution functions of Poisson and binomial distributions.

of the underlying distribution. The first moment of the Poisson distribution is given by its expectation value $\bar{n} = E(\mathcal{N})$, whereas the second central moment is the square root of the expectation value of the squared difference between the random variable and its expectation value $\sigma = \sqrt{E((\mathcal{N} - \bar{n})^2)}$. Hence, no matter what distribution, σ provides a measure of variation, i. e., a measure of noise. As a result, the SNR gives a measure for the signal quality by dividing the expectation value with the second central moment. If the measured data would not contain any noise, σ would be zero and the SNR would approach infinity. If the noise level increases, also σ increases, thus the SNR decreases. The expectation value $\bar{n}$ in the numerator makes the SNR stable to scaling, that means if we measure very high values at the detector a small amount of noise is less critical as if we measure small values that contain the same amount of noise. For X-rays, we can demonstrate that the $SNR(\mathcal{N}) \propto \sqrt{N_0}$ (cf. Geek Box 7.9). As a consequence, SNR only doubles if we use four times as many photons for N_0. Note this estimation is simplified and neglects some effects such as detector read-out noise.

Geek Box 7.3: Poisson Distribution

The Poisson distribution is a discrete probability distribution and its mass distribution function is defined by

$$\text{Poisson}(N_0) = p(\mathcal{N} = n) = \frac{(N_0)^n}{n!}\, e^{-N_0} \quad , \tag{7.7}$$

where N_0 is the expectation value of the observed event $E(\mathcal{N})$. We now show a simple example for the usage of the Poisson distribution. Assume a local shop records its daily number of customers for a year which results in an average of $N_0 = 15$ customers per day. The Poisson distribution can now be used to calculate the probability that on a new day there will be $n = 20$ customers in the shop, i. e., $p(\mathcal{N} = 20) = \frac{(N_0)^n}{n!}\, e^{-N_0} = \frac{15^{20}}{20!}\, e^{-15} \approx 0.0418$. In Fig. 7.18(a), the mass distribution function as defined in Eq. (7.7) is shown for three different expectation values N_0. If the number of N_0 becomes high, the Poisson distribution approaches a normal distribution with mean $\bar{n} = N_0$ and standard deviation $\sigma = \sqrt{N_0}$. This is based on the so called "central limit theorem". In Fig. 7.18(a), we have also added the corresponding mass distribution functions for each Poisson distribution. You can clearly see that the higher N_0, the closer the discrete Poisson distribution gets to a normal distribution.

7.5 X-ray Applications

7.5.1 Radiography

Radiography describes the process of creating two dimensional projection images by exposing an anatomy of interest to X-rays and measuring the attenuation they undergo when passing through the object. It is a very common form of X-ray imaging and is used in clinics around the globe.

The main application area is the examination of fractures and changes of the skeletal system. Here, the high attenuation coefficient of bones compared to the surrounding tissue delivers a good contrast and allows for distinct detection and classification of fractures. Moreover, radiography can be used to detect changes of a bone's consistency or density, e. g., in case of osteoporosis or bone cancer. In Fig. 7.19, two X-ray images of an arm with fractures of Ulna and Radius bones are shown on the left. Furthermore, the figure shows a color image taken from the arm after intervention and also two further X-ray images of the treated arm where the bones have been internally fixated using metal plates.

Geek Box 7.4: Binomial Distribution

The binomial distribution is also a discrete distribution and can be used to model a series of Bernoulli trials, i. e., a series of random experiments with binary outcome. The mass distribution function is given by

$$p(\mathcal{N}=n) = \binom{N}{n} p^n \,(1-p)^{N-n} = \frac{N!}{n!\,(N-n)!}\, p^n \,(1-p)^{N-n} \quad . \tag{7.8}$$

It describes the probability that exactly n positive outcomes occur in a series of N independent trials, where p denotes the probability for an individual trial having a positive outcome. The most intuitive example for a binomial distribution is coin tossing. From coin tossing we know that the probability of getting head or tails in a single toss is "fifty-fifty", i. e., $p = 0.5$. If we now want to know the probability to get exactly $n = 20$ times heads when you toss the coin $N = 30$ times, $p(\mathcal{N}=20) = \binom{N}{n} p^n \,(1-p)^{N-n} = \frac{30!}{20!\,(30-20)!}\,(0.5)^{20}\,(1-0.5)^{30-20} \approx 0.028$. In Fig. 7.18(b), three cases of a binomial mass distribution function are shown for a varying number of trials N. The probability of a single trial being true was fixed with $p = 0.5$.

Geek Box 7.5: Statistics of the X-ray Generation Process

How is the Poisson distribution related to X-ray imaging? It can be shown that the number of generated X-ray photons at the anode is Poisson distributed. As input parameters we have the number of accelerated fast electrons N_e and the probability for one fast electron being converted to an X-ray photon p_{ex}. The distribution is then given by

$$\begin{aligned} N_0 &= N_e\, p_{ex} \\ P(\mathcal{N}=n) &= \frac{(N_e\, p_{ex})^n}{n!}\, e^{-N_e\, p_{ex}} \quad , \end{aligned} \tag{7.9}$$

where N_0 denotes the expected value for the number of electrons that trigger an X-ray photon, which is also known as a measure for the radiation intensity. We use $P(N_x)$ as the probability that an X-ray source produces exactly N_x X-ray photons. $P(N_x)$ is then given by above equation, where n has been replaced by N_x.

Geek Box 7.6: Statistics of the X-ray Matter Interaction

The generated X-ray photons are now traveling through space towards the detector and interact with the matter they pass through according to Beer's law as introduced in Eq. (7.3). Whether the photons interact with the matter or pass through it unaffected can be interpreted as Bernoulli trial, i. e., an experiment with random binary outcome. If a single photon encounters an interaction depends on the material properties along the photons path, i. e., the attenuation $\mu(x)$. The probability p_a for the photon passing unaffected is again given by Beer's law:

$$p_a = e^{-\int \mu(x)\mathrm{d}x} \quad . \tag{7.10}$$

As the individual X-ray photons are independent from each other in terms of interacting or not, the process can be described as a binomial distribution. Furthermore, it can be shown that when we have a Poisson distributed variable (N_x) that represents the number of samples in a binomial distribution, the outcome is again Poisson distributed. We refer to Geek Box 7.7 for further information.

Geek Box 7.7: Combining Poisson and Binomial Distribution

As the individual X-ray photons are independent from each other in terms of interacting or not, the process can be described as a binomial distribution

$$\begin{aligned} P(\mathcal{N} = n_s) &= \sum_{N_x=n_s}^{\infty} P(N_x) \cdot P(n_s|N_x) \\ &= \sum_{N_x=n_s}^{\infty} \frac{(N_0)^{N_x}}{N_x!} e^{-N_0} \cdot \binom{N_x}{n_s} p_a^{n_s} (1-p_a)^{N_x-n_s} \quad , \\ &= \frac{(N_0\, p_a)^{n_s}}{n_s!} e^{-N_0 p_a} \end{aligned}$$

where N_x is the number of X-ray photons, n_s is the number of photons that pass through the object unaffected, $P(N_x)$ is the probability that the X-ray generation produces N_x photons and $P(n_s|N_x)$ is the conditional probability that models the number of unaffected photons, given the number of input photons. The sum comes from the "Law of Total Probability" and is necessary to eliminate the conditional probability. $P(\mathcal{N} = n_s)$ now gives the overall probability that n_s photons will arrive at the detector after having passed the object. We refer to [1, p. 65] for a detailed derivation.

Geek Box 7.8: Probabilistic Lambert-Beer Law

The resulting distribution for the number of photons after matter interaction is thus given by

$$P(\mathcal{N} = n_s) = \frac{(N_0\, p_a)^{n_s}}{n_s!}\, e^{-N_0 p_a} \quad , \tag{7.11}$$

where n_s is the number of photons that pass through the matter unaffected. We can also determine the expectation value of this Poisson distribution, i. e.,

$$E[n_s] = N_0\, p_a = N_0\, e^{-\int \mu(x)\mathrm{d}x} \quad . \tag{7.12}$$

Hence, the expectation value as given by Eq. (7.12) is again Lambert-Beer's law which was introduced in Sec. 7.3.
Note that each process that now follows in the X-ray detection step can also be modeled or at least approximated by a binomial distribution. This holds for the conversion of X-ray photons to light photons in scintillator based detectors, for the subsequent conversion of light photons to electrons but also for the conversion of X-ray's to electrical charges in direct conversion flat panel detectors. Each of these steps yields another Poisson distribution for the number of outgoing photons or electrons, hence also the final value at the end of the detection step follows a Poisson distribution. This observation is crucial, as it tells us that all of the measurements that we get from our detection system follow Poisson distributions including its behavior regarding noise which will be discussed next.

7.5.2 Fluoroscopy

Conventional radiography typically refers to the acquisition of a single or small number of X-ray projection images for a specified view. In contrast, fluoroscopy describes a sequence of radiographic images acquired periodically at a certain frame rate. The X-ray source can either be triggered for each frame or simply provide a constant radiation exposure to the region of interest. Potential X-ray detectors can be image intensifiers (see Sec. 7.4.1) or the newer FPDs (see Sec. 7.4.2). The frame rate is typically limited by the acquisition speed of the detection system. For image intensifiers, it is given by the inertia of the final fluorescent screen, whereas for FPDs it is determined by the speed of the electronic detector readout step. In practice, frame rates of 30 frames per second are possible. However, rates are often reduced for dose reasons.

Geek Box 7.9: Signal to Noise Ratio for X-rays

Let us focus on the distribution for the number of photons that arrive at the detector, i. e., n_s. The distribution is given by Eq. (7.11). From Poisson statistics we know that the expectation value is the only parameter of the mass distribution function, which was already computed in Eq. (7.12), hence, $\bar{n} = N_0\, p_a$. Further, it can be shown that the variance (σ^2) of a Poisson distribution is equal to the expectation value, i. e., $\sigma^2 = N_0\, p_a$. The SNR after photon interaction with the object can then be computed by

$$\begin{aligned} SNR(\mathcal{N}) &= \frac{N_0\, p_a}{\sqrt{N_0\, p_a}} \\ &= \sqrt{N_0\, p_a} \\ &= \sqrt{N_0}\; e^{-\frac{1}{2}\int \mu(x)\mathrm{d}x} \quad . \end{aligned} \tag{7.13}$$

Above equation shows us that the SNR of an X-ray imaging system of course depends on the object, represented by $e^{-\frac{1}{2}\int \mu(x)\mathrm{d}x}$ and also on the number of generated photons at the source N_0. The SNR is proportional to the square root of the number of emitted X-ray photons, hence increasing the number of photons also increases the SNR. However, a higher number of photons also means a higher dose level for the patient which is often the limiting factor and gives an upper bound for the SNR.

Fluoroscopy is of special importance in minimally invasive interventions, where catheters, endoscopes, and other tools need to be guided and operated without direct visual contact to the region where the actual intervention takes place. It is also the key technology for visualizing vessels such as arteries or veins by the use of contrast agent, as described in the following section. In Fig. 7.20(a), an example image from a fluoroscopy sequence is depicted that shows the placement of the two electrodes and wires of a heart pacemaker. A typical clinical setup for a minimally invasive surgery is shown in Fig. 7.20(b), where the X-ray imaging unit is given by a C-arm scanner that can be freely positioned around the patient.

Figure 7.19: Arm showing fractures in radiographic images, the corresponding color image after surgery and the radiographic images after fixation of the bones using metal rods. Image is in public domain and was taken from [11].

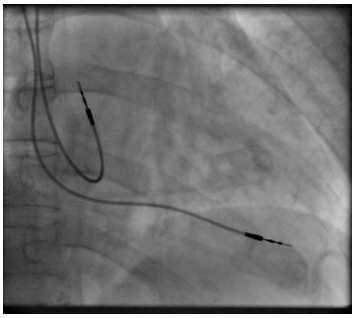

(a) Pacemaker Fluroscopy. Image taken from [5].

(b) Clinical Setup. Image courtesy of Siemens Healthineers AG.

Figure 7.20: Left: Image from a fluoroscopy sequence showing the placement of two electrodes of a pacemaker. Right: Typical clinical setup of a minimally invasive surgery. The fluoroscopy is acquired using a freely positionable C-arm device. The image shows the X-ray source at the bottom and the FPD is right above the patient.

7.5.3 Digital Subtraction Angiography

Angiography refers to the imaging of arteries (venography for veins) to analyze properties such as shape, size, lumen, or flow rate. Usually, the attenuation properties of vessels do not substantially differ from that of the surrounding tissue which makes X-ray-based imaging hard and yields poor contrast.

To increase image quality and contrast often contrast agent is injected into the blood circulation. Contrast agent is a liquid that provides an increased attenuation coefficient compared to normal soft tissue. Typical contrast media

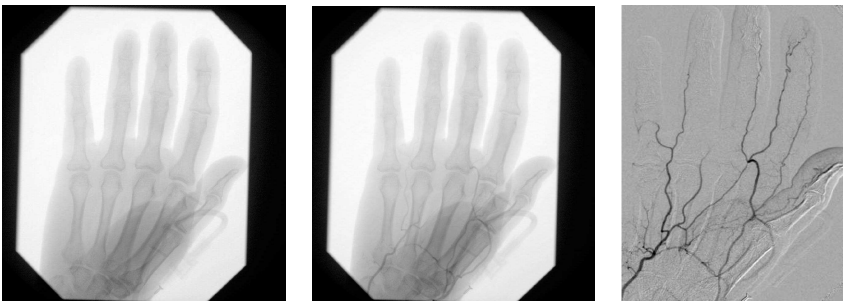

(a) Mask Image **(b)** Fill Image **(c)** Angiogram

Figure 7.21: Process of creating a DSA. In (a) the hand was imaged and no contrast agent has been injected (mask image). In (b) the same hand has been imaged but including injected contrast agent. The difference of (b) and (a) represents the angiogram as shown in Figure (c). Images provided by Adam Galant, Siemens Healthineers AG.

are iodine and barium, where the first is used for intravascular and the latter for gastrointestinal examinations. Thus, iodine is injected into the blood circulation whereas barium can be swallowed to investigate, e. g., the stomach or colon.

In DSA, a fluroscopic sequence of a fixed anatomy is acquired. At the same time contrast agent is injected in regular intervals into the vessel system. X-ray images that have acquired the scene without contrast agent are assumed to show the background tissue that is typically not of interest. If we now subtract the initially acquired background image from an X-ray image with contrast and assume that no patient motion has taken place, we can measure the attenuation caused only by the injected contrast agent. As the contrast agent is limited to the vessel system, it has been injected to, the outcome of such a subtraction will be a visualization of the vessels only. In Fig. 7.21, an example for a DSA acquisition is presented. First the contrast agent free image, i. e., the mask image, is acquired as shown in Fig. 7.21(a). Then contrast is injected into the vascular system and after some waiting a further image, i. e., the fill image, is acquired. The difference of both images is then the so called angiogram that shows only the contributions given by the contrast agent and thus the vessels are visualized (cf. Fig. 7.21(c)).

Further Readings

[1] Thorsten M. Buzug. *Computed Tomography: From Photon Statistics to Modern Cone-Beam CT*. Berlin, Germany: Springer, 2008, p. 536. ISBN: 3642072577.

[2] PM De Groot. “Image intensifier design and specifications”. In: *Proc. Summer School on Specification, Acceptance Testing and Quality Control of Diagnostic X-ray Imaging Equipment* (1994), pp. 429–60.
[3] Olaf Dössel. *Bildgebende Verfahren in der Medizin - Von der Technik zur medizinischen Anwendung*. Vol. 1. Springer Berlin Heidelberg, 2000.
[4] Jeff Fessler. *Lecture Notes / X-ray imaging: noise and SNR*. 2009. URL: http://web.eecs.umich.edu/~fessler/course/516/l/c6-noise.pdf.
[5] Steven Fruitsmaak. *Right atrial and right ventricular leads as visualized under X-ray during a pacemaker implant procedure. The atrial lead is the curved one making a U shape in the upper left part of the figure*. 2008. URL: http://commons.wikimedia.org/wiki/File:Fluoroscopy_pacemaker_leads_right_atrium_ventricle.png (visited on 11/04/2014).
[6] Erich Krestel. “Imaging systems for medical diagnostics”. In: (1980).
[7] Benedikt Lorch et al. “Projection and Reconstruction-Based Noise Filtering Methods in Cone Beam CT”. In: *Bildverarbeitung für die Medizin 2015*. Ed. by H. Handels. Lübeck, 2015, pp. 59–64.
[8] Andreas Maier and Rebecca Fahrig. “GPU Denoising for Computed Tomography”. In: *Graphics Processing Unit-Based High Performance Computing in Radiation Therapy*. Ed. by Xun Jia and Jiang Steve. 1st ed. Vol. 1. Boca Raton, Florida, USA, 2015. ISBN: 978-1-4822-4478-6. DOI: 10.1201/b18968-9.
[9] Andreas Maier et al. “Three-dimensional anisotropic adaptive filtering of projection data for noise reduction in cone beam CT”. In: *Medical Physics* 38.11 (2011), pp. 5896–5909. DOI: 10.1118/1.3633901.
[10] Jihong Wang and Timothy J. Blackburn. “The AAPM/RSNA Physics Tutorial for Residents”. In: *RadioGraphics* 20.5 (2000), pp. 1471–1477.
[11] Wikimedia. *Broken fixed arm*. 2006. URL: http://en.wikipedia.org/wiki/Bone_fracture#mediaviewer/File:Broken_fixed_arm.jpg (visited on 11/04/2014).
[12] Wei Zhao and JA Rowlands. “X-ray imaging using amorphous selenium: Feasibility of a flat panel self-scanned detector for digital radiology”. In: *Medical Physics* 22.10 (1995), pp. 1595–1604.